European Commission
Research Programme of the Research Fund for Coal and Steel

ANGELHY

Innovative solutions for design and strengthening of telecommunications and transmission lattice towers using large angles from high strength steel and hybrid techniques of angles with FRP strips

WORK PACKAGE 3 – DELIVERABLE 3.3

Numerical model validation and parametric study of closely spaced built-up members

Coordinator:

National Technical University of Athens - NTUA, Greece

Beneficiaries:

ArcelorMittal Belval & Differdange SA - AMBD, Luxembourg

Université de Liège - ULG, Belgium

COSMOTE Kinites Tilepikoinonies AE - COSMOTE, Greece

Centre Technique Industriel de la Construction Métallique - CTICM, France

SIKA France SAS - SIKA, France

Grant Agreement Number: 753993

03/12/2020

AUTHORS:

CTICM
Steel Construction Research Division
Espace Technologique – Immeuble Apollo
L'Orme des Merisiers – F-91193 Saint Aubin
Authors: André Beyer, Alain Bureau

Numerical model validation and parametric study of closely spaced built-up members

TABLE OF CONTENTS

1 Introduction

Deliverable 3.3 describes hereafter the validation of the numerical model used for the parametric study on closely spaced built-up members. After the validation of the numerical model, a sensitivity study is presented highlighting the main parameters influencing the member behaviour and resistance. Finally, the scope of the parametric study is presented. The numerical results of the parametric study and the development of the design procedure are detailed in deliverable D3.4 of ANGELHY.

In the following three configurations are considered for the study of closely spaced built-up members:

1) **Back-to-back connected angles** (noted as BBE – see Figure 1.1a)
2) **Star battened angles with equal sections** (noted as SBE – see Figure 1.1b)
3) **Star battened angles with unequal sections** (noted as SBU – see Figure 1.1c)

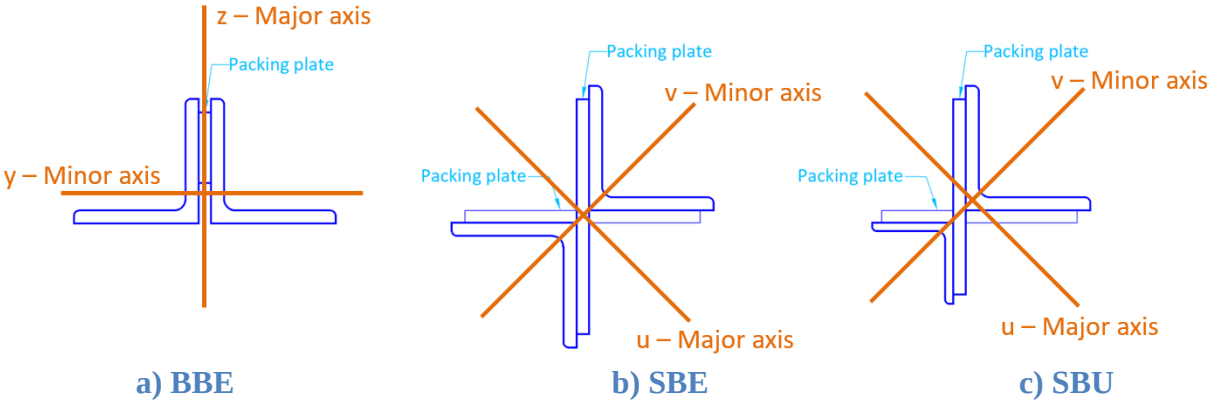

Figure 1.1: Typology of closely spaced built-up members to be tested

2 General presentation of the numerical model

The numerical simulations are performed with the program ANSYS version 18.2. In order to simulate as precisely as possible the behaviour of the laboratory tests, the numerical analysis is based on a model with solid element "Solid 186" of the ANSYS element library. This element possesses 20 nodes (8 nodes on the summit and 12 mid-side nodes) with three degrees of freedom (displacements about the x-, y- and z-axis). "Solid 186" supports plasticity, large deflection and large strain as well as initial stress state (residual stresses) and is therefore capable to simulate precisely the behaviour of steel sections. It should be noted that one single bolt per packing plate is used for specimens of type BBE whereas two bolts have to be used per packing plate for specimens of type SBE and SBU as shown in Figure 2.2.
In Figure 2.1 and Figure 2.2, the angle sections are welded onto two endplates. This type of boundary condition is used to recalculate the laboratory tests. In the framework of the parametrical study, the angle sections are connected through gusset plates at their end as shown in Figure 2.3.

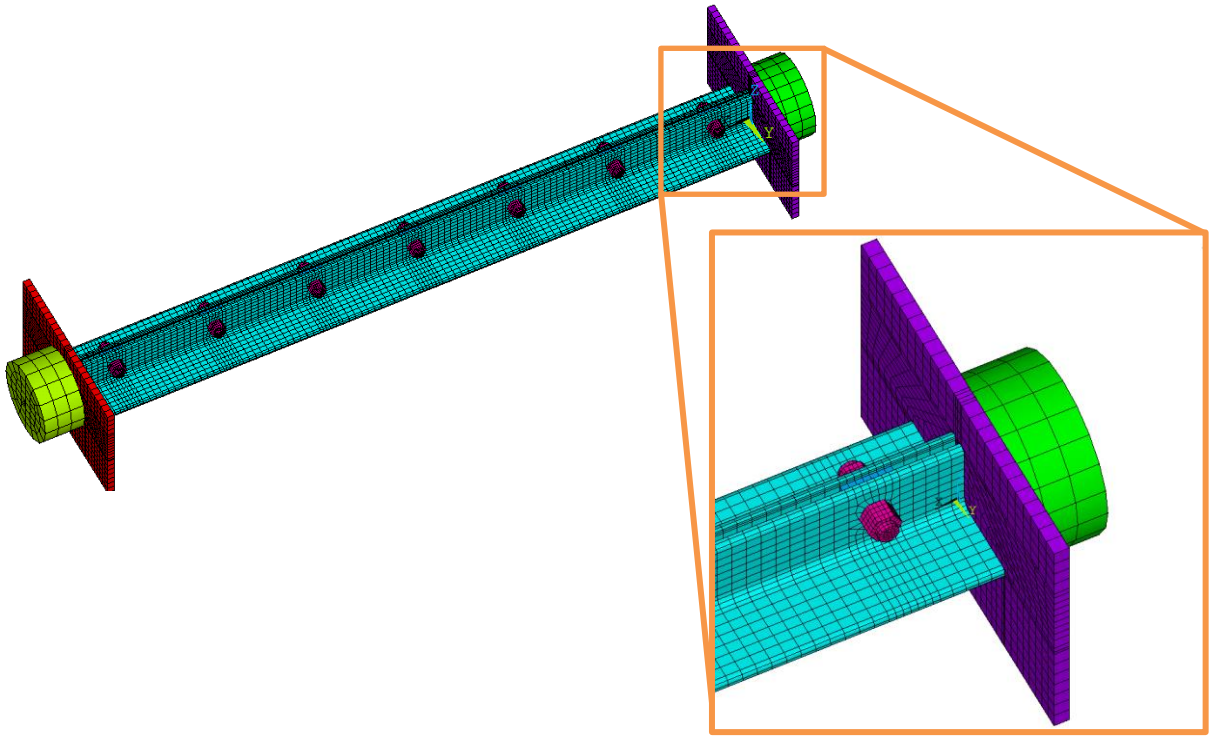

Figure 2.1: Global view of the numerical model used for the preliminary analysis of the test specimens

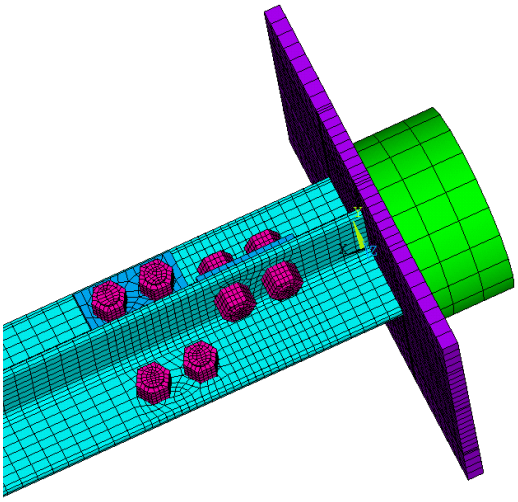

Figure 2.2 : Detailed view of load introduction for a specimen of type SBE

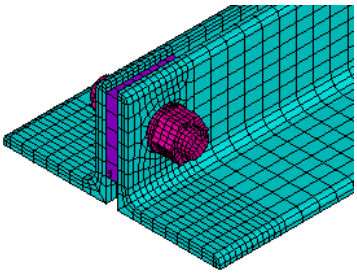

Figure 2.3 : Detailed view of load introduction through gusset plate for the parametric study

In order to represent the real stiffness of the built-up section, several contact regions have to be defined. These regions are presented in Figure 2.4 for BBE specimens. The same principal applies for SBE and SBU specimens. For the contact between the nut and the angle sections and the one between the packing plates and the angle sections a friction coefficient of 0.2 is applied.

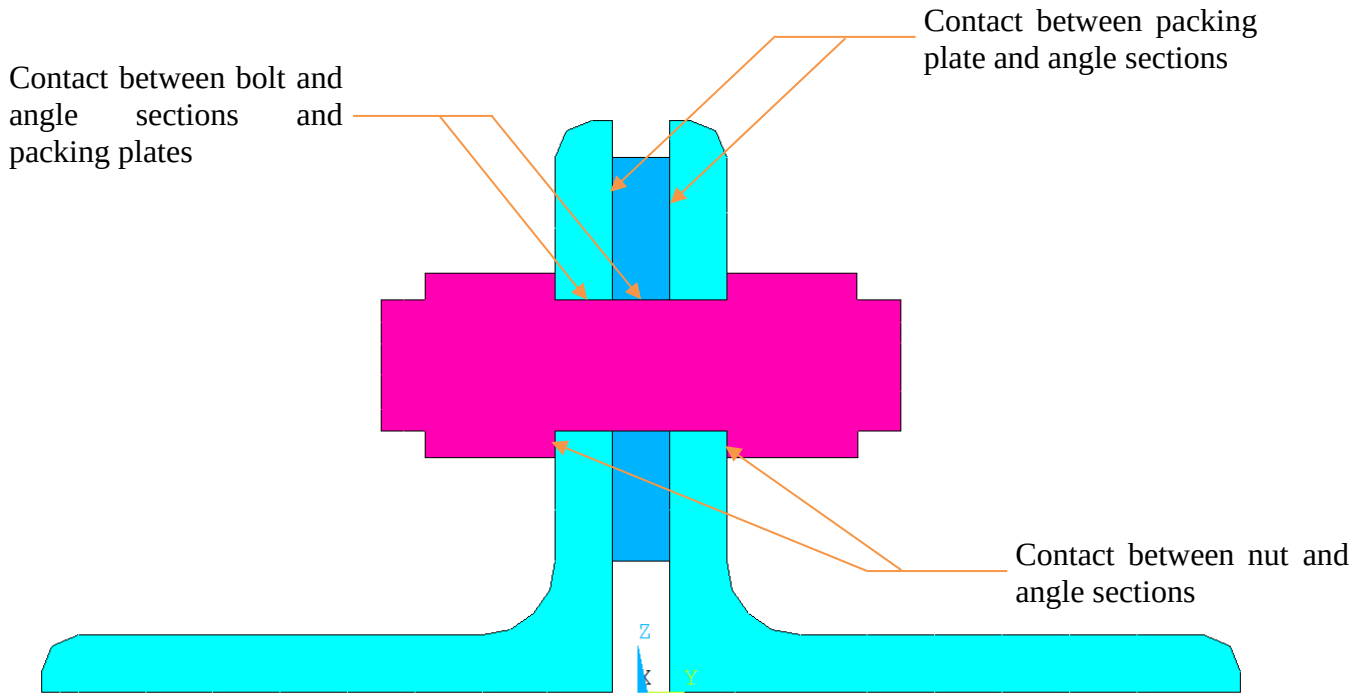

Figure 2.4: Contact regions in the built-up member

The specific assumptions concerning the imperfection and material properties are presented in the following paragraphs.

3 Validation of the numerical study through ANGELHY laboratory tests

3.1 Specific assumptions on boundary conditions and imperfections

The laboratory tests performed in the framework of ANGELHY are presented in detail in deliverable 3.2. Hereafter, the numerical model is confronted to these tests accounting for the measured material law, measured geometric dimensions and imperfections and the residual stress model of Figure 3.1.

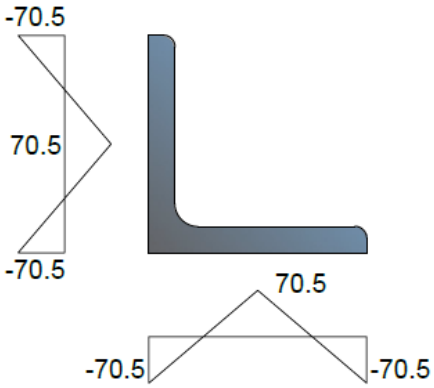

Figure 3.1: Residual stress model [2]

The boundary conditions applied in the numerical model, schematically represented in Figure 3.2, are based on the design used in the laboratory (see deliverable 3.2 for more details).
It should be noted that in case of SBE and SBU sections, the rotations about the y (noted $w_{,x}$ and z axis (noted $v_{,x}$) are free whereas the rotation about the y axis is fully restrained ($w_{,x} = 0$) as shown in Figure 3.2. Figure 3.2 also indicates that the load is introduced by an imposed axial displacement *u* applied at one member end. At this end, the torsional twist φ is also restrained in the numerical simulations to avoid numerical instabilities (at least one restraint concerning the rotation about the longitudinal axis is necessary). At the member ends, the boundary conditions are applied at the node situated at the centre of the cylinder represented in green colour. This node is then linked by the MPC contact technology of ANSYS to the other nodes situated on the outer circular surface of the cylinder. This avoids stress peaks potentially generated by the local application of the boundary conditions.

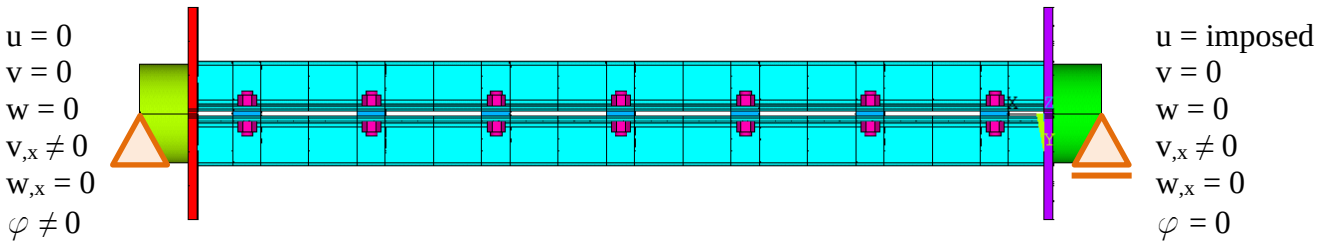

Figure 3.2: Schematic representation of the boundary conditions for the numerical simulations

3.2 General results

Table 3.1 shows a first comparison between the numerical simulations and the laboratory tests. One may clearly observe that many results obtained through the numerical simulations are very conservative. Only in case of SBU specimens, the numerical model appears to be suitable to represent the behaviour of the laboratory specimens. Additionally, it appears that in case of BBE and SBE specimens, the failure mode is generally not well represented by the numerical model. In case of SBU specimens, both the laboratory test specimens and the numerical specimens fail by an interaction of major axis bending and major axis buckling.

Table 3.1: Comparison between laboratory tests and numerical simulations

Test	Experimental results		Numerical simulation		P_{Num}/P_{Exp}
	Failure mode	Failure load P_{Exp} (kN)	Failure mode	Failure load P_{Num} (kN)	
BBE1	CS/Fby	678,56	Fby	615,11	0,91
BBE2	Fbz	485,36	Fby	248,01	0,51
BBE3	Fby	601,61	Fby	459,99	0,82
BBE4	Fby	311,68	Fby	245,06	0,79
BBE5	Fbz	423,32	Fby	251,94	0,60
BBE6	Fbz	382,78	Fby	211,20	0,55
SBE1	Fb	346,83	Fb	255,99	0,74
SBE2	Fb	296,32	Fb	152,24	0,51
SBE3	Fb	283,10	Fb	150,84	0,53
SBE4	Fb	127,41	Fb	88,92	0,70
SBE5	Fb	251,92	Fb	152,90	0,61
SBE6	Fb	81,47	Fb	85,30	1,05
SBU1	Fb	231,97	Fb	222,05	0,96
SBU2	Fb	168,26	Fb	160,94	0,96
SBU3	Fb	152,54	Fb	142,45	0,93
SBU4	Fb	84,68	Fb	87,10	1,03

3.3 Detailed results for SBU specimens

Table 3.1 indicates that the numerical model yields very satisfactory results compared to the laboratory tests in terms of failure load, for SBU specimens. The following figures (Figure 3.3 for specimen SBU 1 and Figure 3.4 for specimen SBU 2) represent the load displacement plots for specimens SBU 1 (member length = 2200 mm, 2 intermediate packing plates) and SBU 2 (member length = 3000 mm, 3 intermediate packing plates). In these figures the reaction force

is represented as a function of measured displacements. Both figures clearly show that the numerical model represents well the behaviour of the tested specimens.

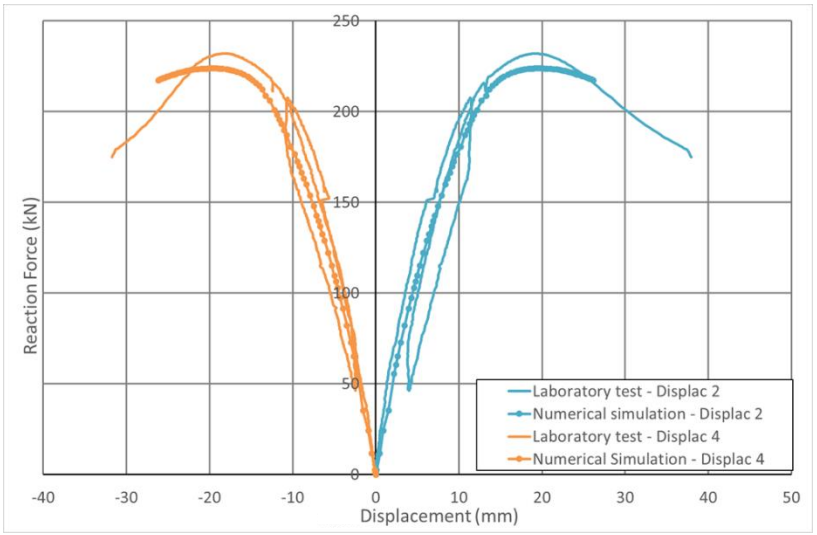

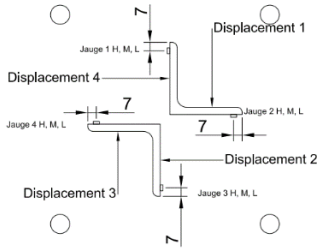

a) b)

Figure 3.3: a) Load displacement paths for specimen SBU 1 and b) definition of displacements

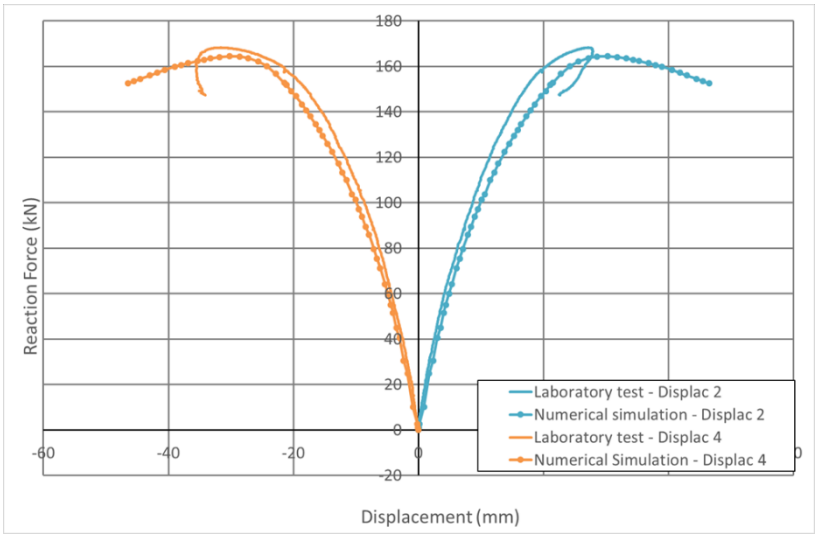

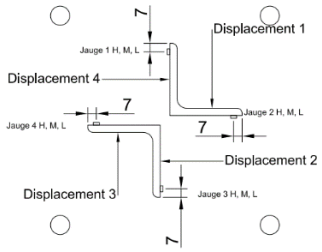

a) b)

Figure 3.4: a) Load displacement paths for specimen SBU 2 and b) definition of displacements

3.4 Detailed results for BBE and SBE specimens

The observations for BBE and SBE specimens are similar. Therefore, the following discussions focus on BBE specimens. First, the experimentally obtained load displacements paths are recalled in Figure 3.5 to Figure 3.7 (for more details see Deliverable 3.2). It should also be recalled that the specimens whose results are represented hereafter failed by minor axis

buckling even though major axis buckling has been expected as natural failure mode owing to the boundary conditions ($N_{cr,z} < N_{cr,y}$ – see Figure 1.1 for the definition of axis – z indicates here the major axis). Also, the failure loads exceeded the minimum critical axial force associated to the expected failure mode. Yet, the failure load is even lower than the critical axial force linked to observed failure mode.

The following three figures indicate the same general behaviour. The displacements resulting from the applied load and imperfections are very low. Then at a given load level, the member fails abruptly as indicated by the highly increasing displacements M2 and M3 (indicating minor axis flexural buckling). The behaviour indicates therefore bifurcation rather than divergence generally observed for imperfect columns.

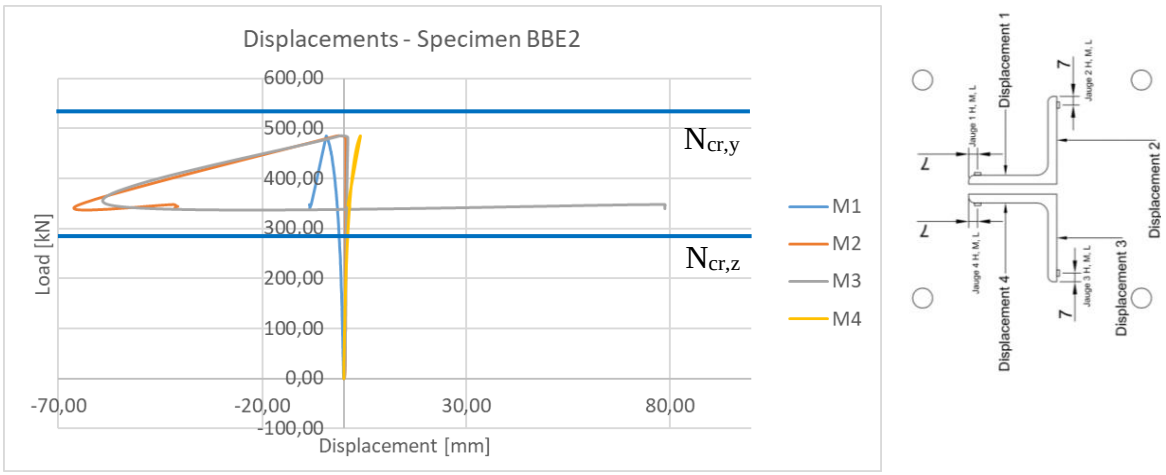

a) b)

Figure 3.5: a) Load displacement paths for specimen BBE 2 and b) definition of displacements

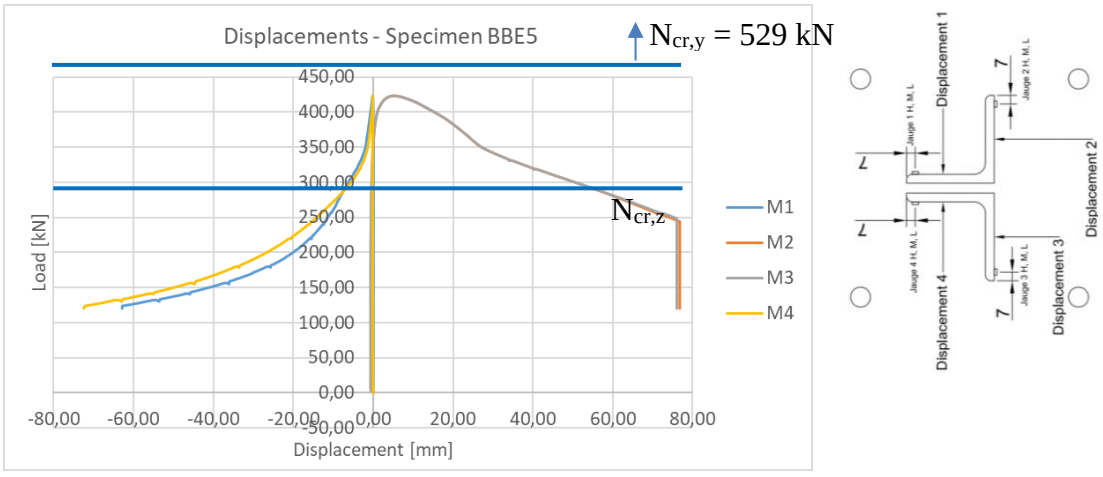

a) b)

Figure 3.6: a) Load displacement paths for specimen BBE 5 and b) definition of displacements

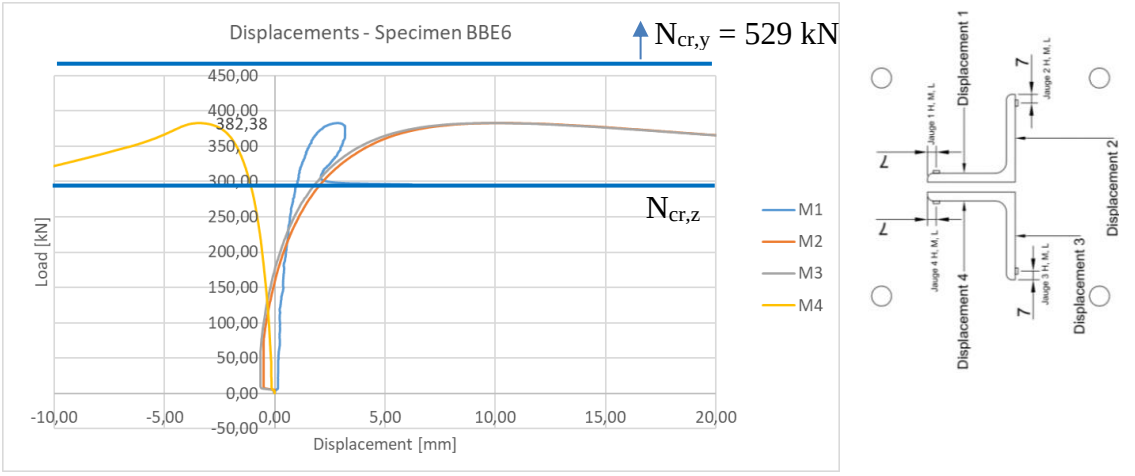

a) b)

Figure 3.7: a) Load displacement paths for specimen BBE 6 and b) definition of displacements

At this point, it seems interesting to recall the measured imperfections for the two specimens represented in Figure 3.5 to Figure 3.7. Figure 3.8 shows first the measurement of the geometric imperfection and positions A (imperfection about minor axis) and B (imperfection about major axis – natural buckling axis owing to boundary conditions).

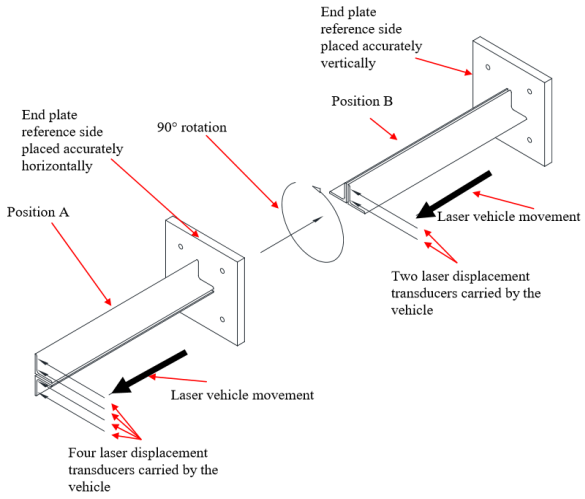

Figure 3.8: Measurement of geometric imperfections

In Figure 3.9 to Figure 3.11, it may be observed that the geometric imperfections about the minor axis are generally higher than those about the major axis. Furthermore, for specimen BBE5, the geometric imperfection about the major axis corresponds to a full sine wave for which the pre-deformation vanishes at mid span leading to a more favourable situation as for an imperfection affine to a half sine wave possessing its amplitude at mid span. One may also note that the geometric imperfection amplitudes are all much lower than L/1000 (3.6 mm). Finally, as the measurements have been performed before the member has been installed in the testing rig, the generation of an additional deformation cannot be excluded.

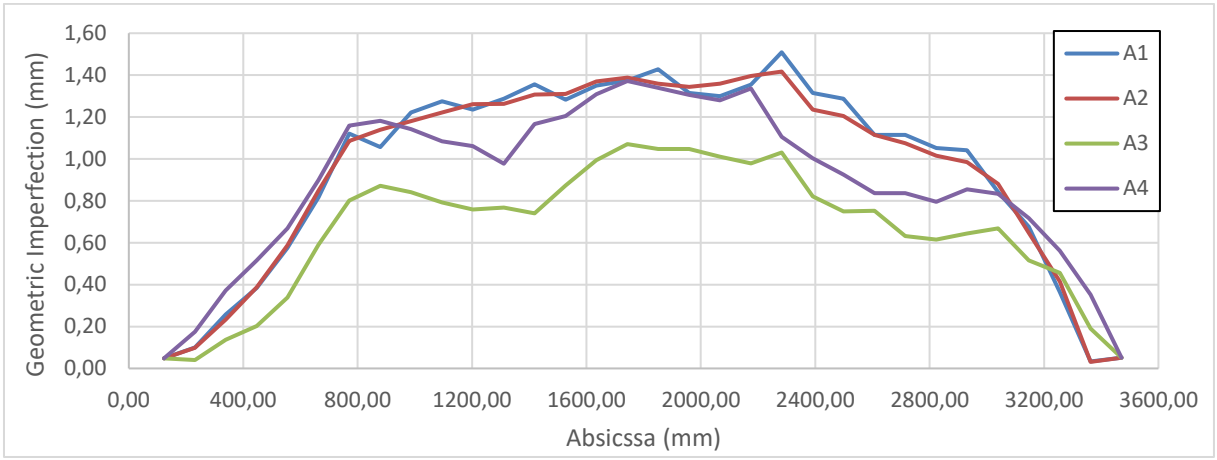

a)

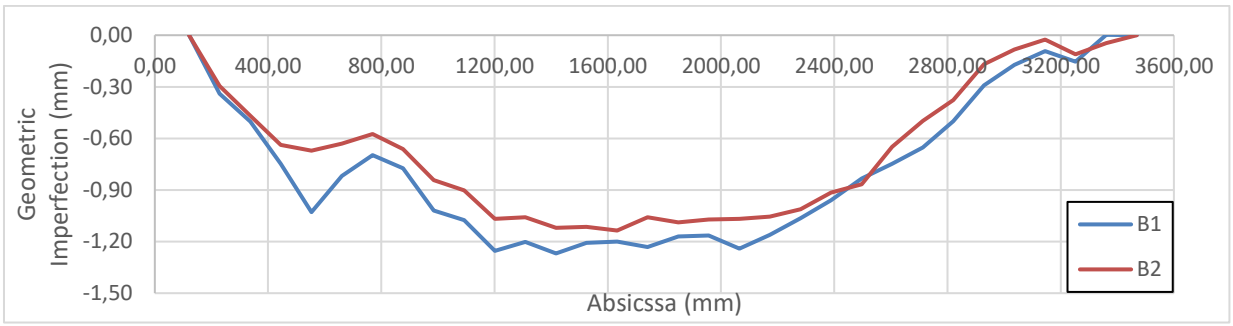

b)

Figure 3.9: Geometric imperfection for BBE2 a) about minor axis and b) about major axis

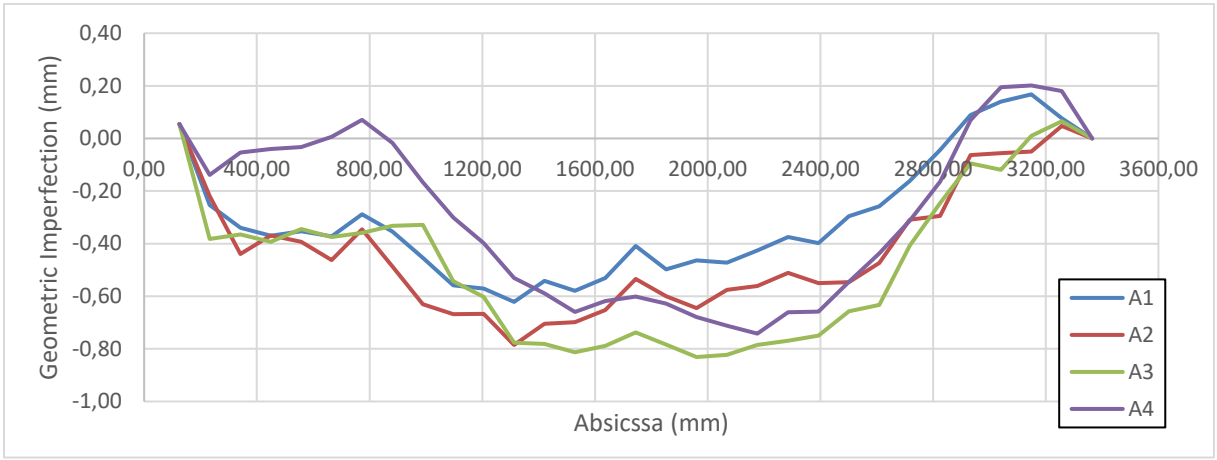

a)

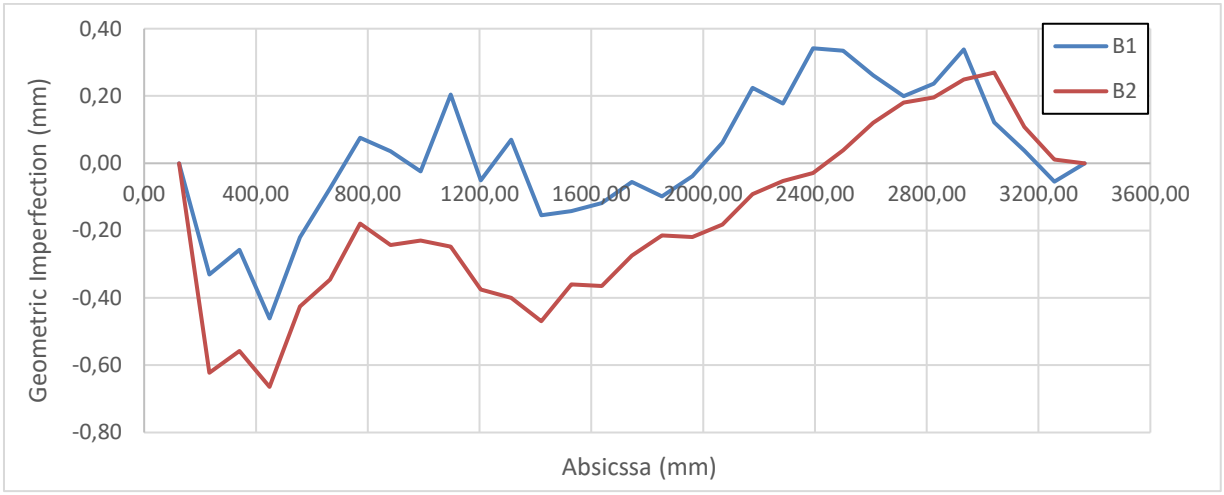

b)

Figure 3.10: Geometric imperfection for BBE5 a) about minor axis and b) about major axis

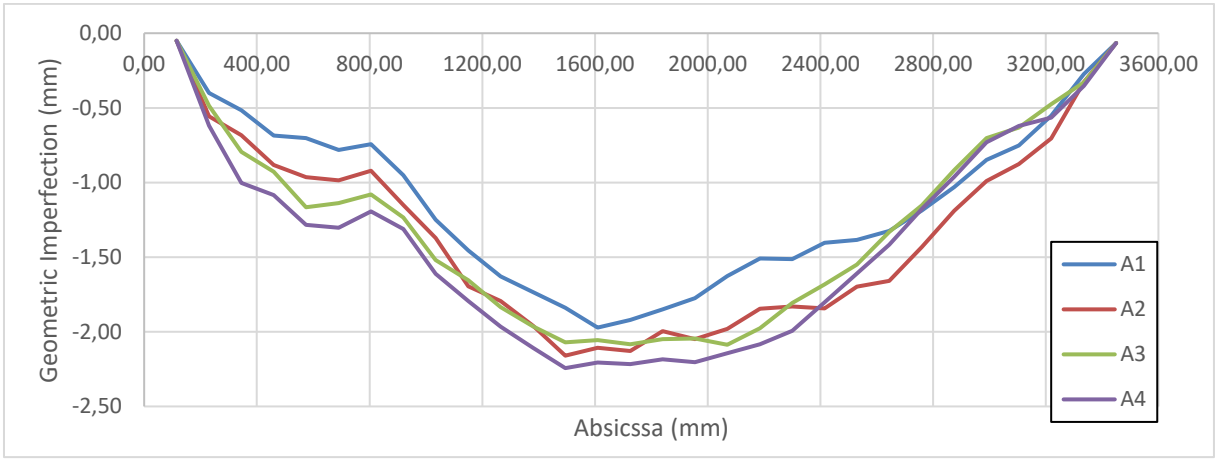

a)

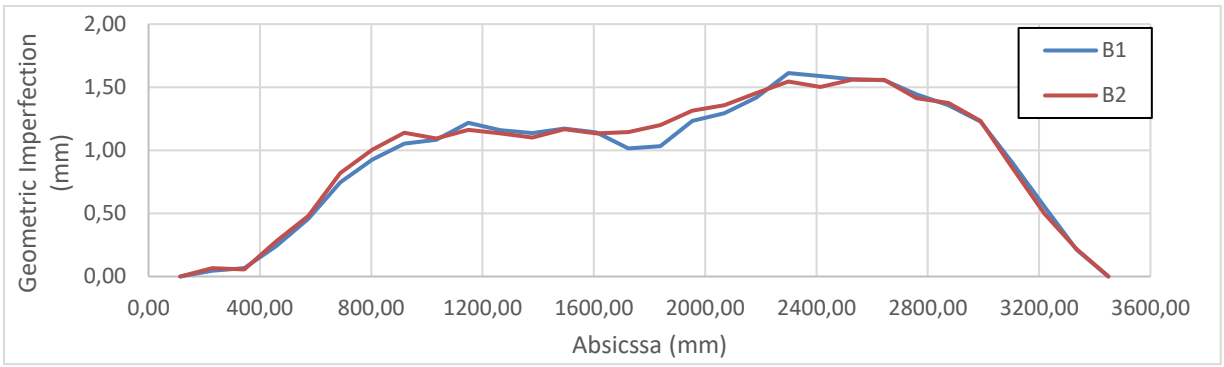

b)

Figure 3.11: Geometric imperfection for BBE6 a) about minor axis and b) about major axis

It appears that the geometric imperfections are more favourable than generally assumed. However, the numerical simulation based on a classical Newton-Raphson approach with implicit integration scheme will not be capable to provide axial forces higher than the minimum critical force. An explicit integration scheme could be applied to study the member behaviour beyond the critical axial force. Here, it is chosen to apply the "Stabilization" approach proposed by ANSYS. The conceptual idea of "Stabilization" is that a spring is added to each degree of freedom in the structure. Consequently, additional stiffness is added to the numerical model. Obviously, the stiffness of these fictitious elements should be as small as possible. This stiffness is controlled through the "energy dissipation ratio". This is a ratio of the work done by the stabilization forces to the element potential energy. In the following, this ratio is chosen equal to 10^{-4}.

Figure 3.12 shows the results that have been obtained for specimen BBE 6 using stabilisation. One may first observe that the numerical results also indicate a failure load higher than the minimum critical axial force. Additionally, the load displacement paths seem to be similar. Also, one may observe that both, the numerical simulation and the laboratory test indicate abrupt failure by bifurcation for the tested specimen. Nonetheless, the numerical simulation is still conservative by about 12%.

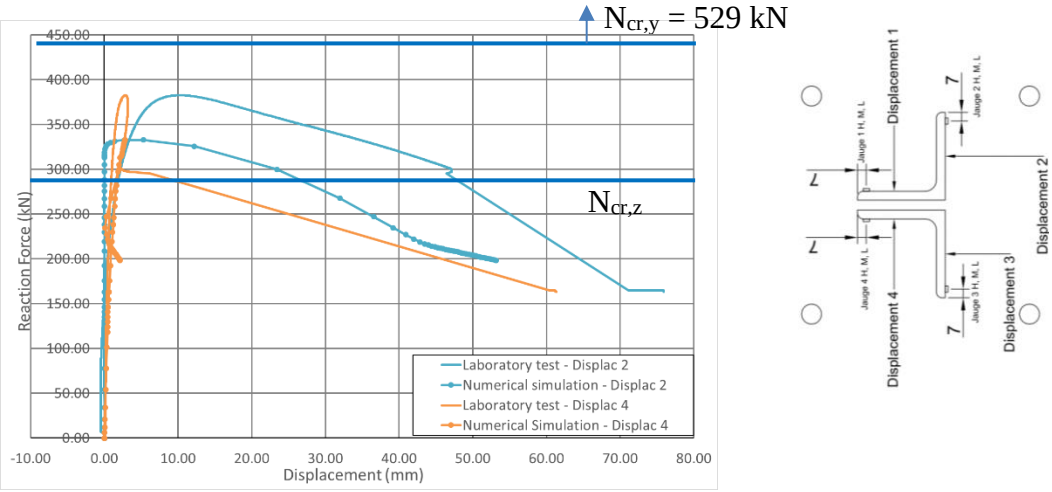

Figure 3.12: a) Load displacement paths for specimen BBE 6 using "stabilization" and b) definition of displacements

Next, it is important to evaluate the amount of work done by the fictitious "springs" in order to stabilize the system. Figure 3.13 compares this work and the strain energy in the member. Clearly, the fictitious work necessary to stabilize the member for buckling about the major axis is fully negligible compared to the strain energy. This indicates that the numerical stabilization does not change the physical behaviour of the member. In fact, only the numerical instability, resulting from the classical implicit integration scheme, is eliminated. Depending on the geometric imperfection, the failure mode may be different from the first eigen buckling mode. Consequently, the failure load can also excess the critical axial load linked to the first eigen mode.

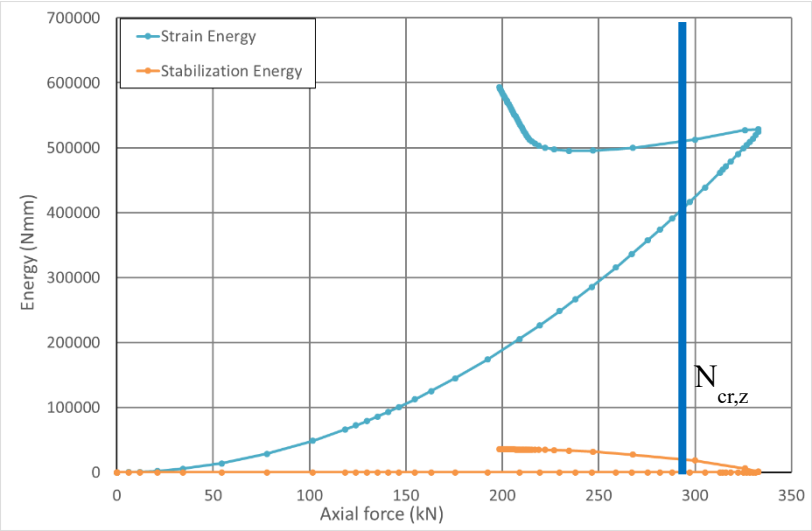

Figure 3.13: Stabilization energy (work done by the "springs") and strain energy of the member

The investigations using the "stabilization" technique revealed that the numerical model may be adapted to fit more precisely the laboratory tests. However, this possibility is not exploited hereafter for several reasons:

- The numerical model is capable to represent the lower bound axial resistance attained by the member if it is subjected to an interaction between bending and axial force as has been shown by the comparison the BBU tests.
- The upper bound resistance highly depends on imperfections and can only be attained by the member if these imperfections are sufficiently favourable. Obviously, this cannot be ensured for all members in practice. Therefore, it is not safe and desirable to exploit the upper bound resistance throughout the parametric study.

4 Validation of the numerical study through laboratory tests from the literature

In reference [1], Kitipornchai et al. reported tests similar to the ones performed in the framework of ANGELHY. However, only back-to-back connected angle sections have been tested. In order to generate a clamped connection about the weak axis, Kitipornchai et al. designed the end connection as shown in Figure 4.1. Nonetheless, the modelling of the support conditions in the numerical model is kept identical to Figure 3.2.

The numerical model considers the cross-section dimensions and the yield stress reported in reference [1]. However, this reference does not provide the value of the geometric imperfection. It only states that "the initial crookedness of all specimens was within commercial tolerances". In the numerical model, a geometric imperfection of L/1000 is therefore applied over both axes. In addition to the geometric imperfection, the residual stress pattern of Figure 3.1 is applied.

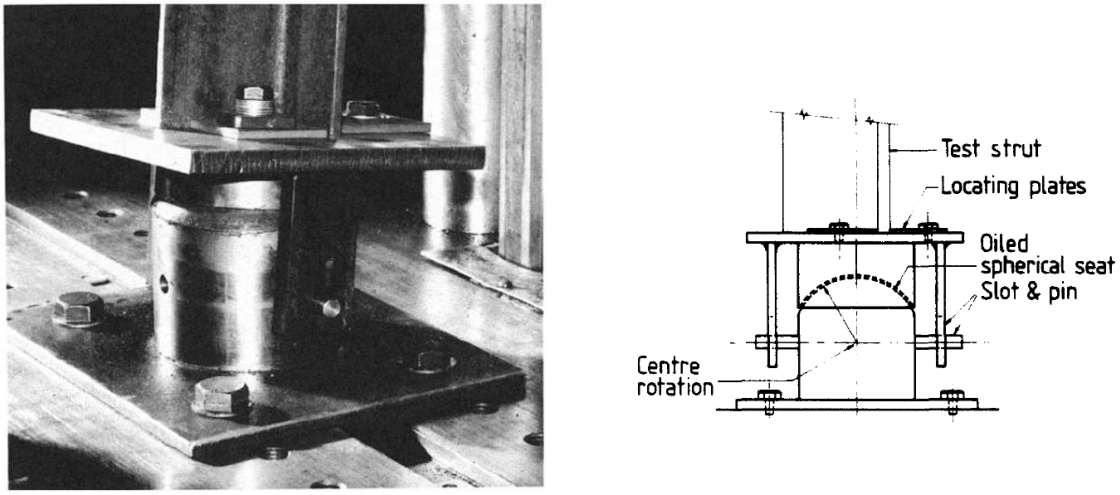

a) Photo of ongoing test **b) Schematic view of support conditions**

Figure 4.1: Support conditions designed in reference (Kitipornchai et al. 1986)

The main parameters of the laboratory tests are summarised in Table 4.1 and the comparison between the results obtained in the laboratory and by the numerical simulations is provided in Table 4.2.

Table 4.1: Laboratory tests performed by Kitipornchai et al. [1]

Test	Cross-section	Length (mm)	Measured properties			
			Leg width (mm)	Thickness (mm)	Yield strength (MPa)	Young's modulus (MPa)
DA1-a.b	2 L51x51x3	1185	50,9	3,2	314	214 000*
DA2-a.b	2 L57x57x5	985	58,2	4,8	268	
DA3-a.b	2 L64x64x5	1185	64,2	4,8	281	
DA4-a.b	2 L76x76x5	1685	76,3	4,8	276	
DA5-a.b	2 L89x89x6.5	1685	88,4	6,4	261	
DA6-a.b	2 L102x102x6.5	1685	100,6	6,5	260	

* Mean value

In Table 4.2, one may observe that the numerical simulations accounting for a geometrical imperfection of sinusoidal shape and amplitude of L/1000 are very close to the laboratory test results. Additionally, the bolt preloading has only little influence on the numerical results as has been shown in the sensitivity study presented in 5.2. One may also observe that the numerical simulations are generally rationally safe sided apart from test DA1-a.b. The resistance of this test is slightly over predicted by the numerical simulations.

Table 4.2: Comparison between laboratory tests of [1] and numerical simulations

Test	Laboratory test		Numerical simulation			
	Failure mode	Failure load P_{Lab} (kN)	Bolts with 50% of nominal preloading		Bolts with 100% of nominal preloading	
			Failure load P_{Num} (kN)	P_{Num}/ P_{Lab}	Failure load P_{Num} (kN)	P_{Num}/ P_{Lab}
DA1-a.b	F	144	154,0	1,09	156,8	1,09
DA2-a.b	F	272	254,1	0,93	254,3	0,94
DA3-a.b	F	312	288,9	0,93	288,9	0,93
DA4-a.b	P	341	312,3	0,92	312,8	0,92
DA5-a.b	F	533	486,7	0,91	486,2	0,91
DA6-a.b	P	636	578,1	0,91	577,3	0,91

F: flexural buckling; P: plate buckling

The following figures represent the load-displacement graphs as well as the von Mises stress distribution at failure. For tests DA4-a.b and DA6-a.b the von Mises stresses are also represented on the displaced member after the peak load in order to represent the failure mode (see Figure 4.6 and Figure 4.9). In Figure 4.6 and Figure 4.9, one may identify local plate buckling. Yet, obviously, the member has also displaced laterally. Therefore, it seems difficult to separate clearly the effect of local (plate) buckling and flexural buckling. Still, in general, the failure modes seem to be well captured by the numerical model.

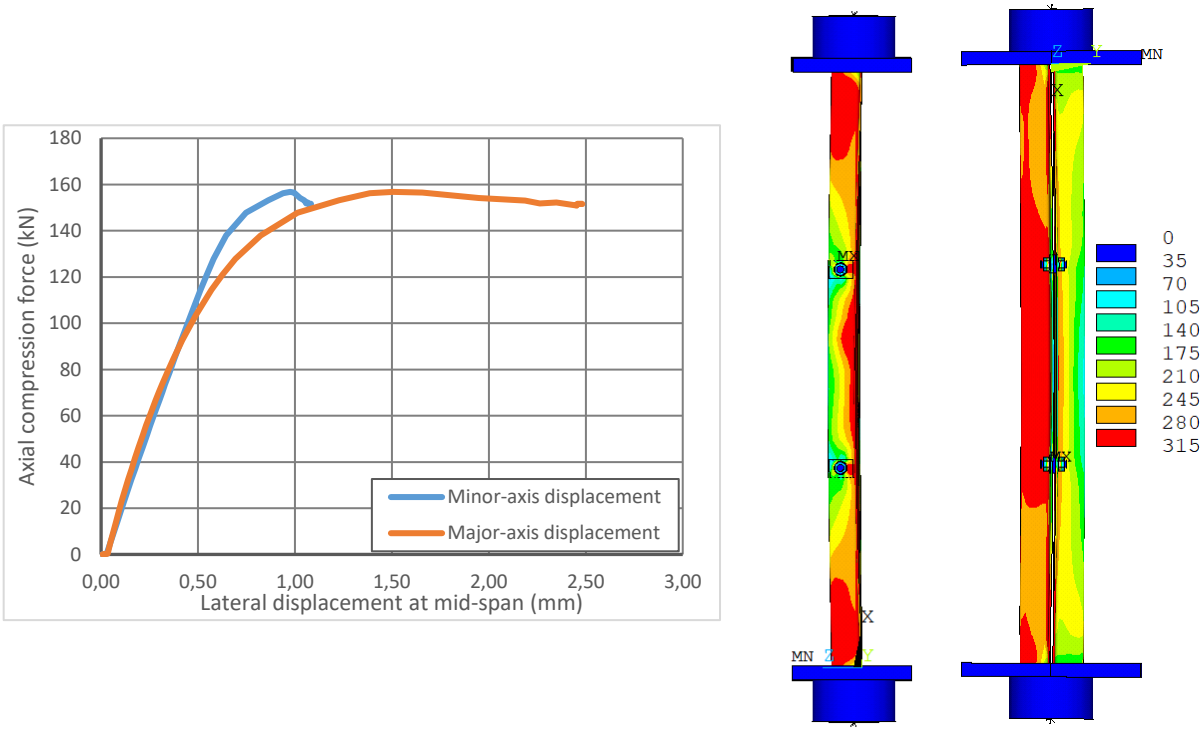

a) Load-Displacement curve b) von Mises stresses (MPa)

Figure 4.2: Results for Test DA1-a.b

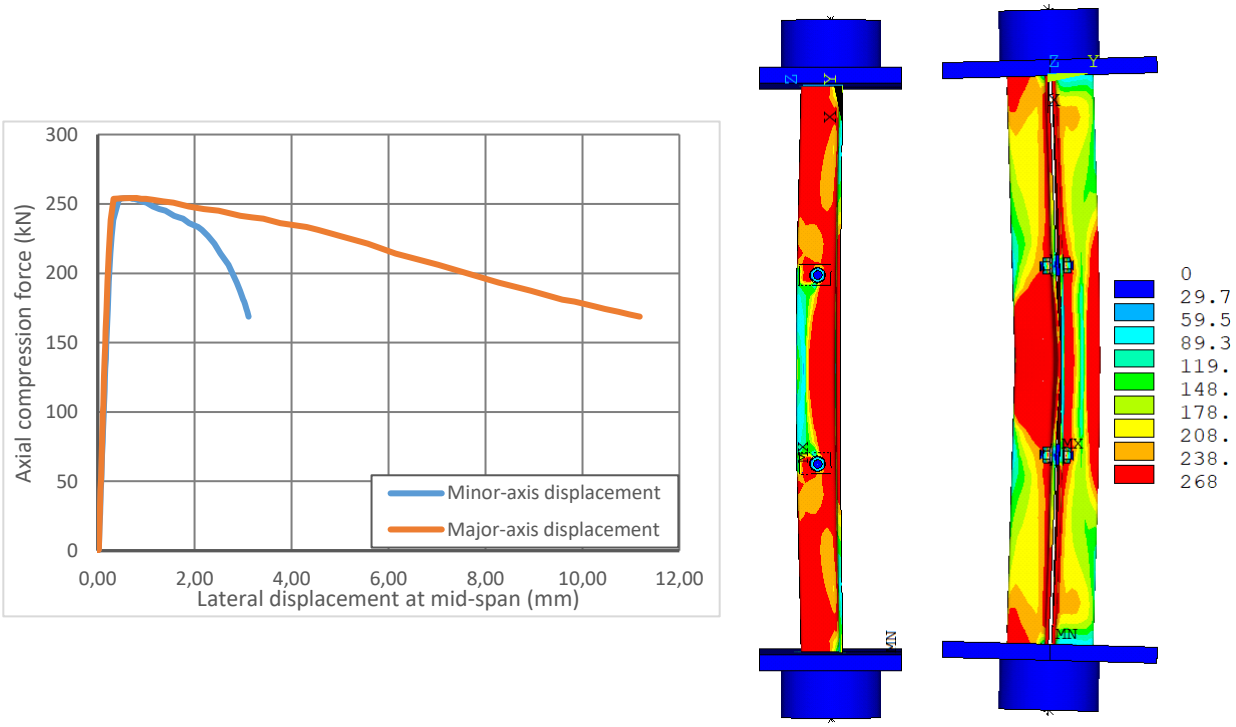

a) Load-Displacement curve b) von Mises stresses (MPa)

Figure 4.3: Results for Test DA2-a.b

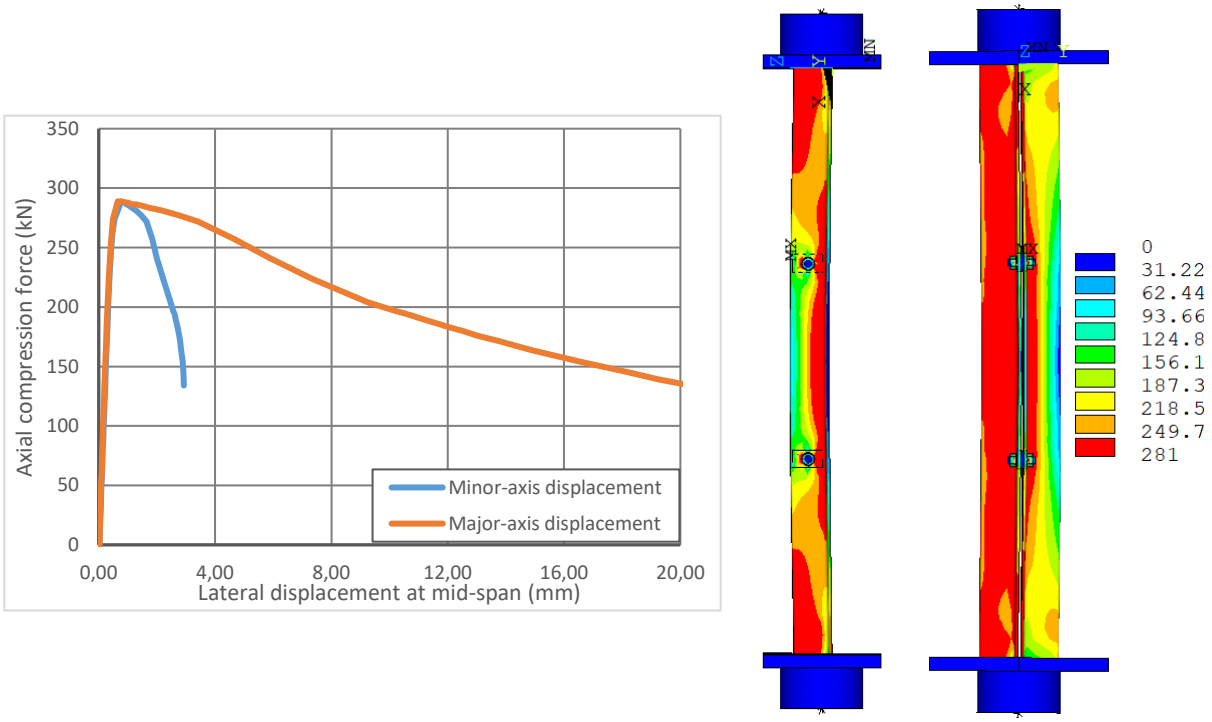

a) Load-Displacement curve b) von Mises stresses (MPa)

Figure 4.4: Results for Test DA3-a.b

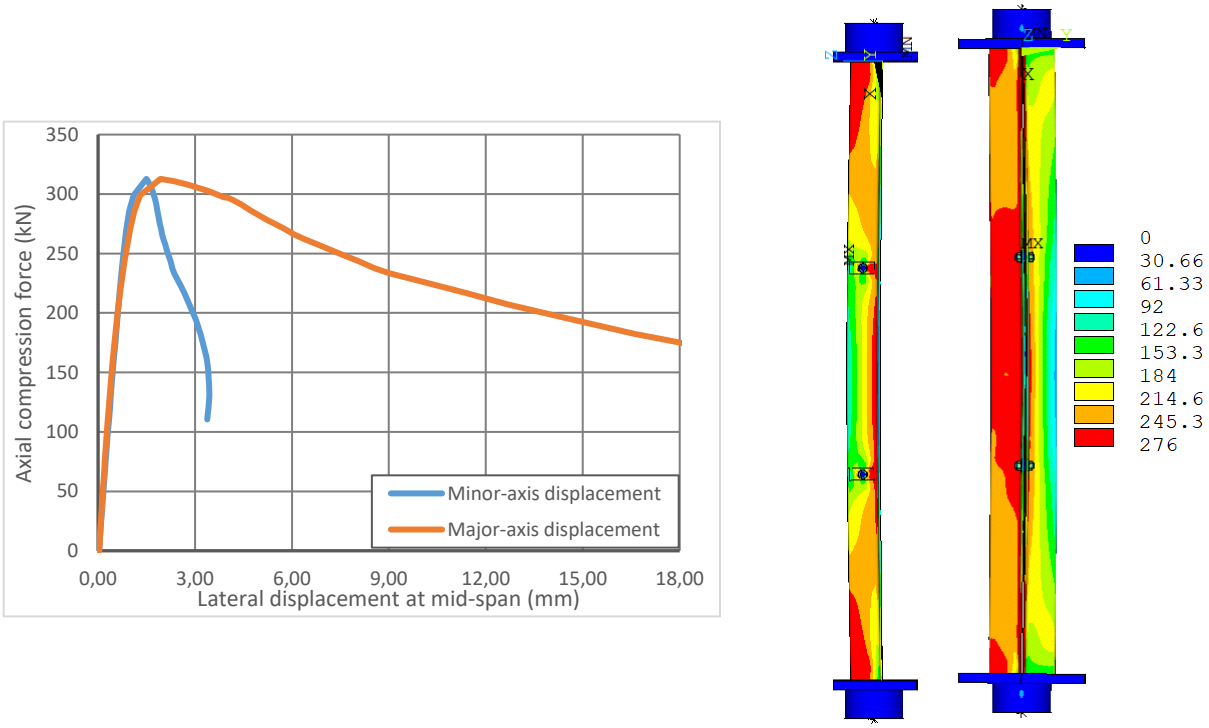

a) Load-Displacement curve b) von Mises stresses (MPa)

Figure 4.5: Results for Test DA4-a.b

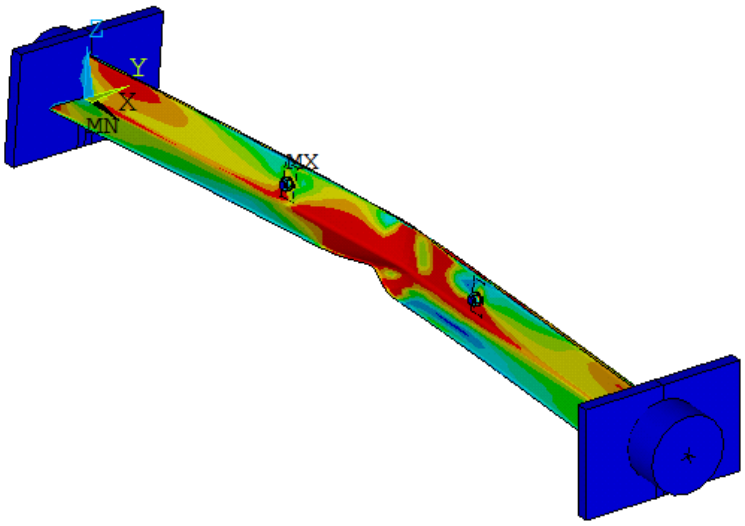

Figure 4.6: Von Mises stresses DA4-a.b at v = 34 mm – Local buckling

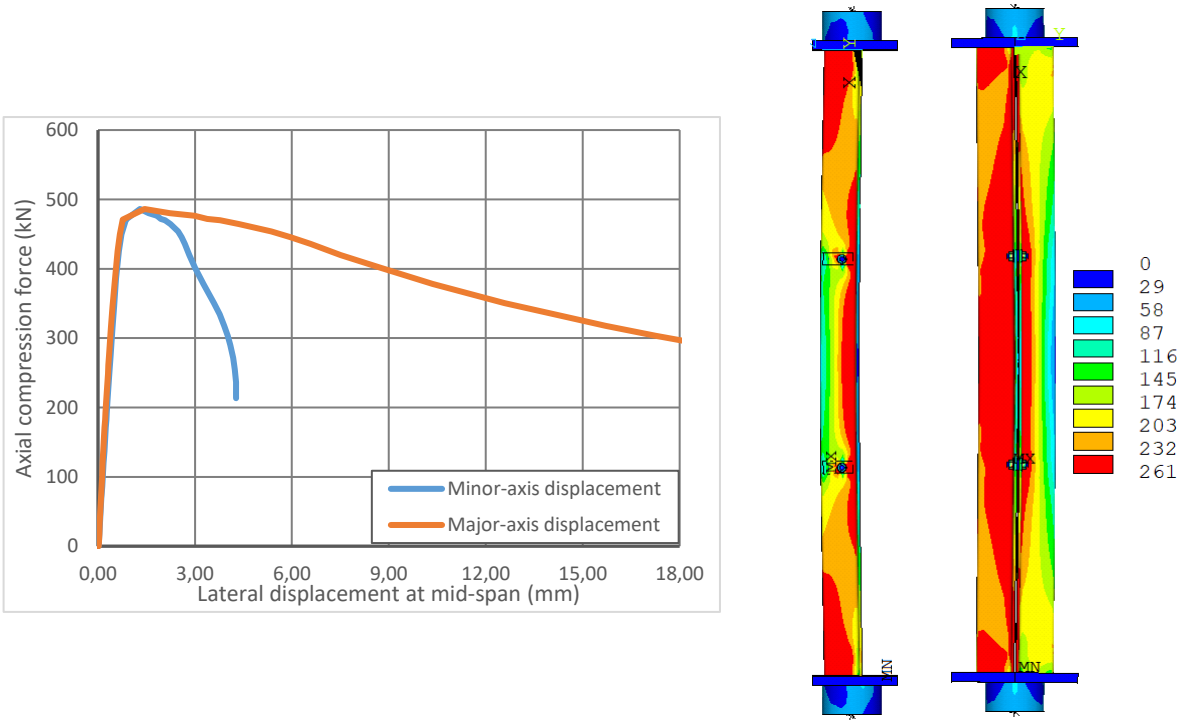

a) Load-Displacement curve b) von Mises stresses (MPa)

Figure 4.7: Results for Test DA5-a.b

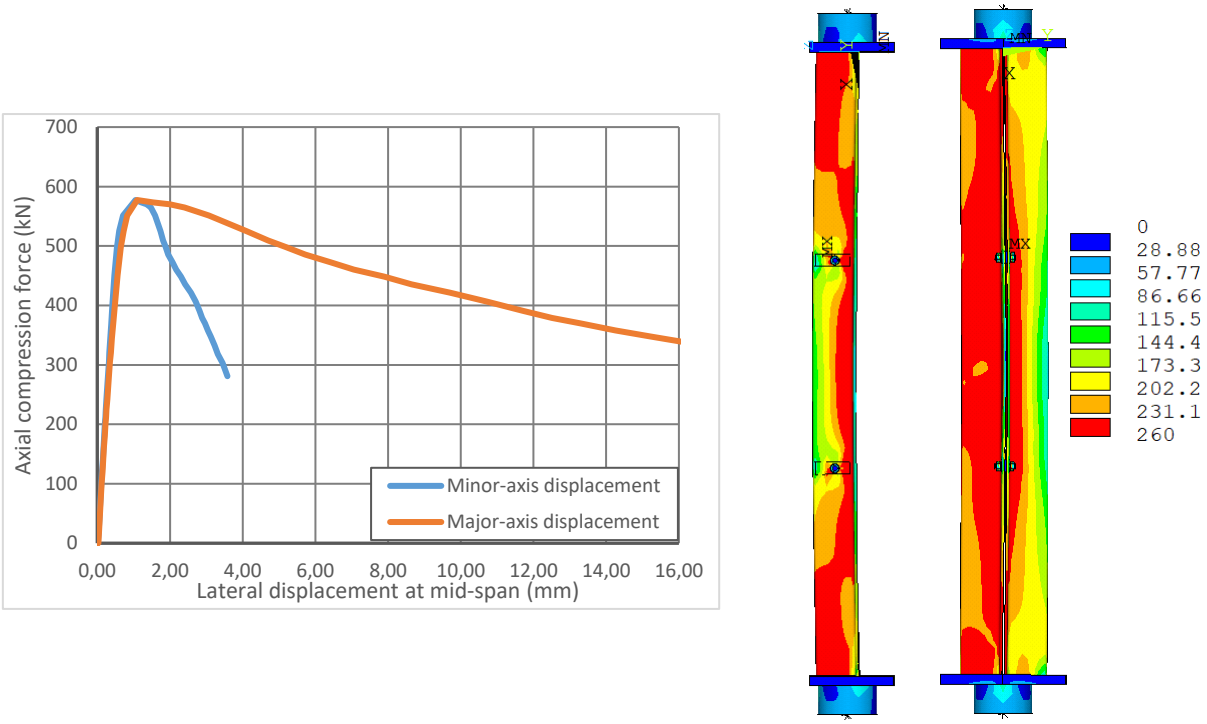

a) Load-Displacement curve b) von Mises stresses (MPa)

Figure 4.8: Results for Test DA6-a.b

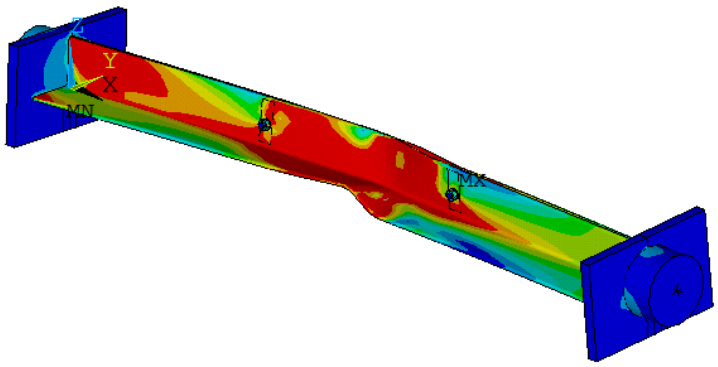

Figure 4.9: Von Mises stresses test DA6-a.b at v = 23 mm – Local buckling

5 Parametric study

5.1 Common assumptions for all configurations

Hereafter, the numerical simulations are presented. For these simulations, the following conventional assumptions are considered:

- Elastic-perfectly plastic material law according to Figure 5.1;
- Geometric imperfection with an amplitude of L/1000 according to the buckling Eigen mode;
- Residual stress pattern according to Figure 3.1.

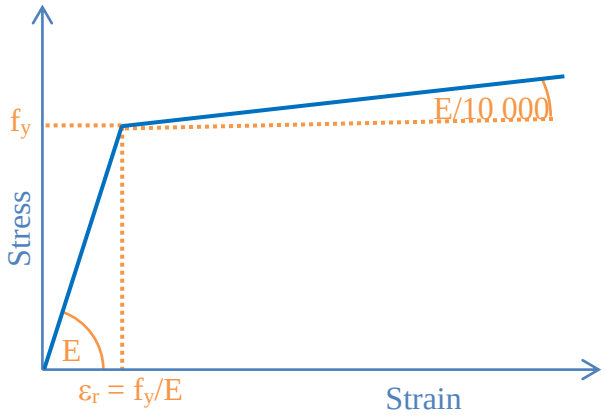

Figure 5.1: Bi-linear stress-strain curved used for preliminary study of the laboratory tests

In all cases, the loads are introduced through an imposed displacement at one member end.

5.2 Sensitivity study

In order to orient the parametric study performed to develop a new resistance model for closely spaced built-up members, this section presents first the results of a sensitivity study. The major aim of this study is the identification of key parameters influencing the resistance. In the framework of the sensitivity study, only BBE specimens are considered.

In the following, the results of geometric and material non-linear analyses including imperfections will be presented in form of force-displacement curves. These diagrams, also provide the theoretical flexural buckling resistance N_b calculated for perfectly connected chords (shear stiffness is assumed to be infinite).

This theoretical value has been calculated based on the critical axial force resulting from the assumption concerning the connection behaviour for buckling about the z-axis and with the European buckling curve b applicable for single angles.

5.2.1 Connection type

First, the influence of the connection type is studied. Three cases are considered:

- Members with welded packing plates.
- Members with non-preloaded bolted connections without any clearance (noted “no Clear” in Figure 5.2).
- Members with non-preloaded bolted connections with a clearance of 2 mm (noted “with Clear” in Figure 5.2). In this case, the bolt hole diameter is equal to the bolt diameter + 2 mm.

Finally, one may note that all connection types are calculated with 4 and with 8 intermediate packing plates. Figure 5.2, representing the results of the numerical simulations, indicates that: The clearance highly reduces the buckling resistance independently from the number of packing plates studied here. Due to the clearance, the shear stiffness of the connection is highly reduced. Members with bolted packing plates and fitted bolts nearly attain the same resistance as members with welded packing plates. Nonetheless, a slight reduction owing to the flexibility of the bolts may be identified.
It appears that members connected with welded or fitted bolted packing plates, whose distance is equal to $30i_{min}$, attain approximatively the theoretical resistance of a single uniform member.

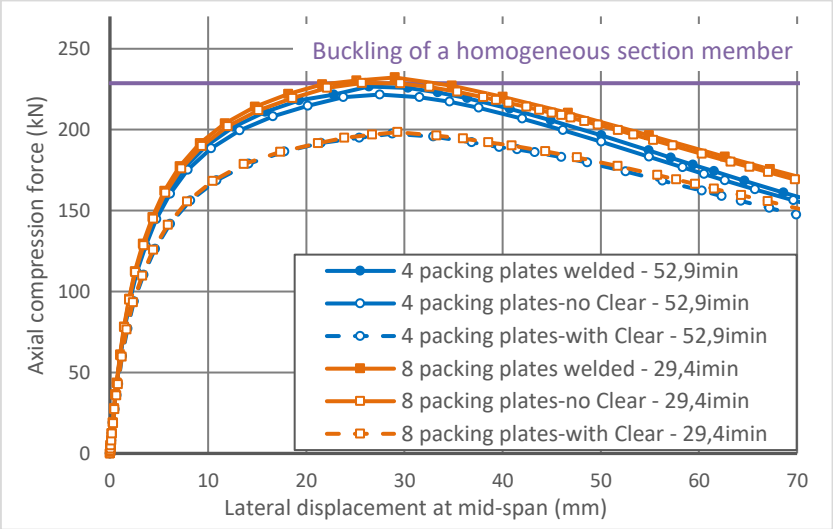

Figure 5.2: Influence of the connection type

5.2.2 Influence of the packing plate spacing

Next, the influence of the number of packing plates (and therefore the distance between the packing plates) is studied. Additionally, it is studied whether the number of packing plates has an influence on the buckling resistance reduction caused by hole clearance for bolted packing plates.
First, the load displacement curves for members with welded packing plates are represented in Figure 5.3. This figure shows that most of the members attain the theoretical buckling resistance of the homogeneous section member. However, the buckling resistance is slightly reduced (approximatively 7%), if only 2 intermediate packing plates are used. Yet, the resulting packing plate spacing of $88i_{min}$ is very high and generally not used in practice.

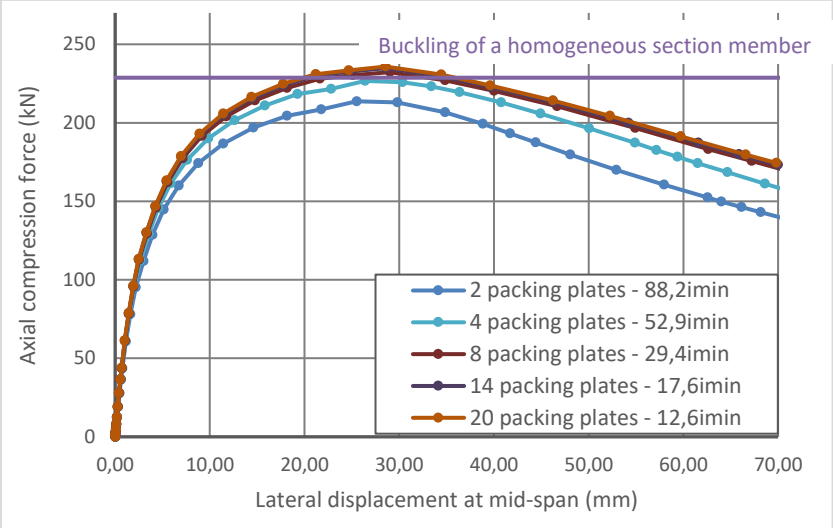

Figure 5.3: Influence of the packing plate spacing – welded connections

Next, Figure 5.4 presents the results for built-up members without hole clearance. If one compares this figure with Figure 5.3, one may observe that the obtained resistances are similar to members with welded connection. Still, it appears that the flexibility of the bolt and the chords between them leads to a slight buckling strength reduction. The difference is of about 2%. Additionally, it appears that for the studied case, a distance of approximatively $30i_{min}$ between packing plates should not be exceeded in order to attain the buckling resistance of the homogeneous section member. In case of welded packing plates, a slightly higher spacing ($40i_{min}$-$50i_{min}$) could be accepted. For higher distances, the reduction of the buckling resistance cannot be neglected anymore. For the studied case, the resistance for the member with only two intermediate packing plates is reduced by approximatively 12% compared to the member with 20 intermediate packing plates.

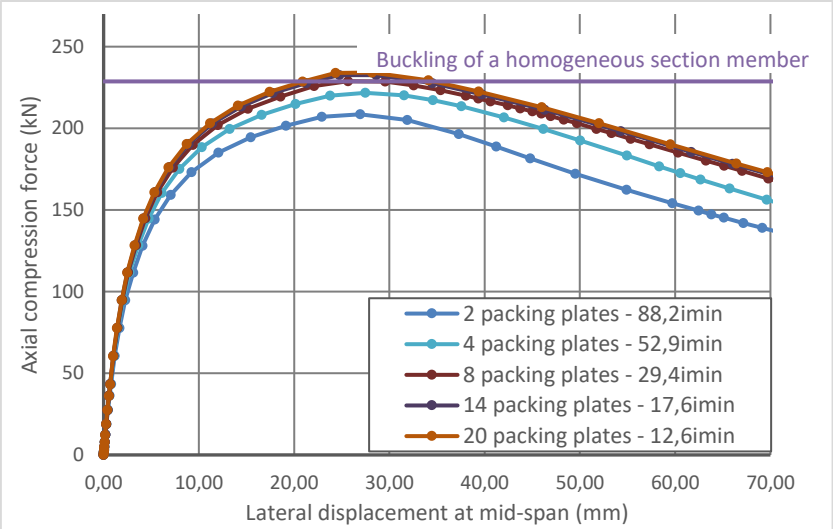

Figure 5.4: Influence of the packing plate spacing – bolted connections without clearance

In case of built-up members possessing a clearance of 2 mm, the distance between the packing plates appears to have only little (or even no) influence on the buckling resistance. In fact, Figure 5.5 shows that the peak load attained by all members is approximatively equal to 195 kN.

It seems that the shear stiffness of the connection completely vanishes owing to the clearance. Therefore, **increasing the number of packing plates does not have any influence on the resistance**. The value of 195 kN appears to be a lower bound value for the studied member.

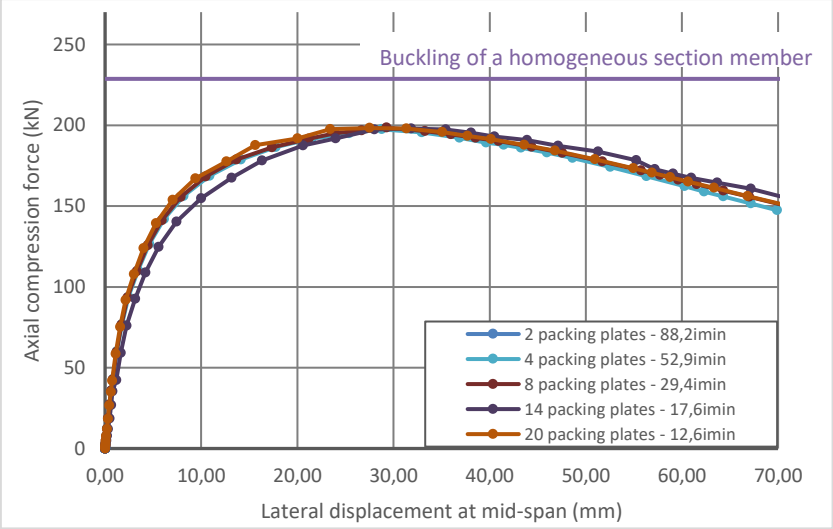

Figure 5.5: Influence of the packing plate spacing – bolted connections with 2 mm clearance

5.2.3 Influence of the clearance

Next, the influence of the value of the bolt hole clearance is highlighted. Figure 5.6 represents results for members with 2 or 20 intermediate packing plates and with respectively, i) no clearance, ii) a clearance of 0.2 mm, iii) a clearance of 0.5 mm and iv) a clearance of 1 mm. One may observe that:

- The results for a clearance of 0.5 mm and of 1 mm are identical for both packing plate arrangements.
- Even a clearance of 0.2 mm leads to a significant reduction of buckling resistance.
- The differences in buckling resistances are higher for members with 20 packing plates than for members with only 2 intermediate packing plates.

The last observation may be easily explained by the fact that the high distance between packing plates already leads to a significant reduction of the buckling resistance. Consequently, a supplementary reduction of the shear stiffness of an individual packing plate connection has less influence on the final resistance. It can be noted again that a lower bound resistance is attained for the studied member at a value of around 195 kN. In case of members connected with a higher number of packing plates, the shear stiffness reduction of each individual packing plate leads to a noticeable strength reduction.

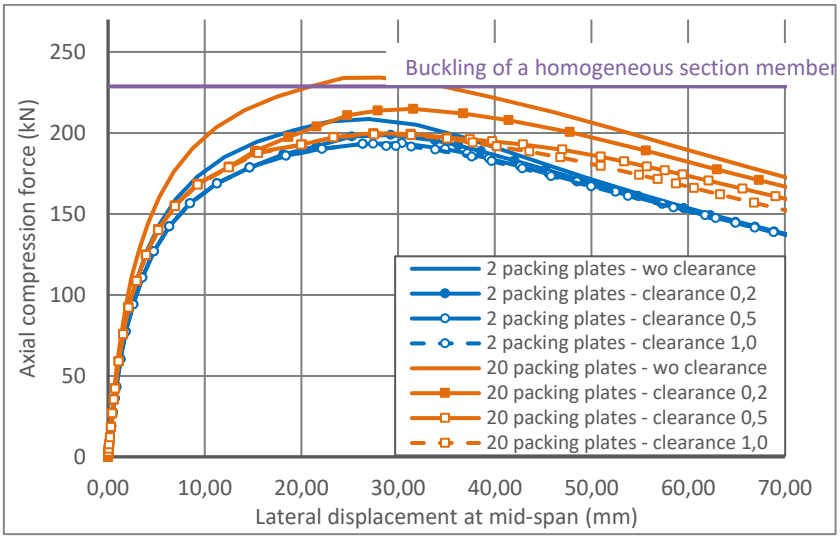

Figure 5.6: Influence of the bolt hole clearance

In order to discuss the influence of the clearance in more details, it is interesting to have a deeper look into the numerical results. Figure 5.8 and Figure 5.9 represent the numerical results for the connection highlighted in Figure 5.7. In particular, the contact status between the bolt and the angle sections is represented. First, Figure 5.8 shows the results of the connection possessing a clearance of 0.5 mm. In Figure 5.9, the clearance is reduced to 0.2 mm.

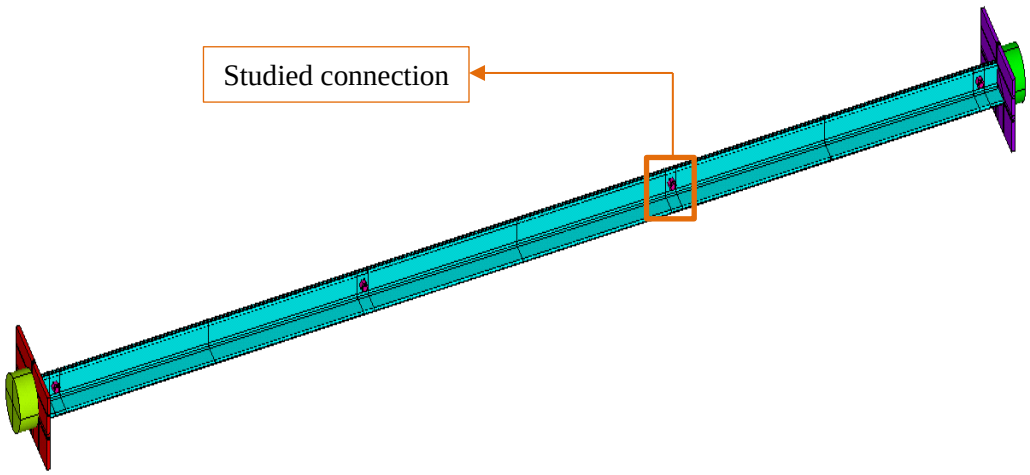

Figure 5.7: Studied member and connection

Figure 5.8 indicates that the bolt shaft is not in contact with the angle section even for a high load level compared to the peak load. In fact, up to an applied load of 185.9 kN (= 96% of the peak load), the bolt shaft is not in contact with the angle sections (the status “NearContact” indicates that the contact is checked numerically but contact has not been detected). The contact is initiated at the peak load level (see Figure 5.8c). Nonetheless, at this late stage, the contact is not capable to increase the stiffness of the member and the failure is initiated.

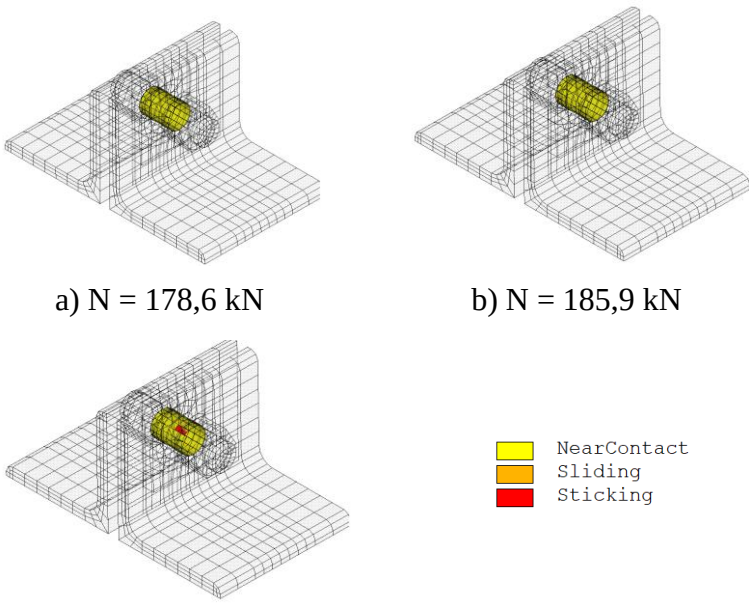

a) N = 178,6 kN b) N = 185,9 kN

c) N = 193,6 kN – Peak load

Figure 5.8: Member with two intermediate packing plates and clearance of 0.5 mm

Next, Figure 5.9 shows the results for the member analysed with a bolt hole clearance of 0.2 mm. Figure 5.9a represents the contact status for an applied load of 178.6 kN. For this axial force the load-displacement curves represented in Figure 5.6 overlap (compare solid blue curve with filled circles and solid blue line with hollow circles). As the contact has not been initiated neither for the case of 0.2 mm clearance nor for the case of 0.5 mm clearance, it is understandable that the member behaviour is identical. Starting from an applied load of approximatively 186 kN, contact is initiated for the connections with 0.2 mm clearance (see Figure 5.9b). As the member has not reached its peak load, the contact – even if rather small – is capable to increase the stiffness of the member. It may be noted that the contact is approximatively perpendicular to the loading direction and consequently a force can be transmitted. The contact shown in Figure 5.8c is nearly parallel to the loading direction. This observation may also explain that the stiffness of the member with 0.5 mm connection clearance is not remarkably increased by the generation of the contact between the bolt shaft and the angle sections.

The effect of the contact between the bolt and the angle sections for members with 0.2 mm clearance can be observed in the load displacement curve of Figure 5.10. As stated before, the stiffness of the member is slightly increased also leading to a slightly increased peak load compared to the member with 0.5 mm clearance (+3%). For members with 0.5 mm clearance the contact, initiated at the peak load level, does not have any noticeable effect on the load displacement curve.

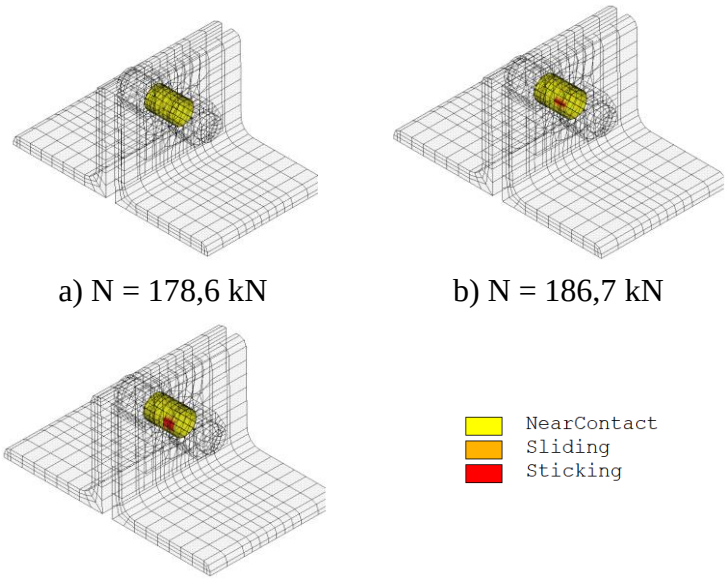

a) N = 178,6 kN b) N = 186,7 kN

c) N = 198,7 kN– Peak load

Figure 5.9: Member with two intermediate packing plates and clearance of 0.2 mm

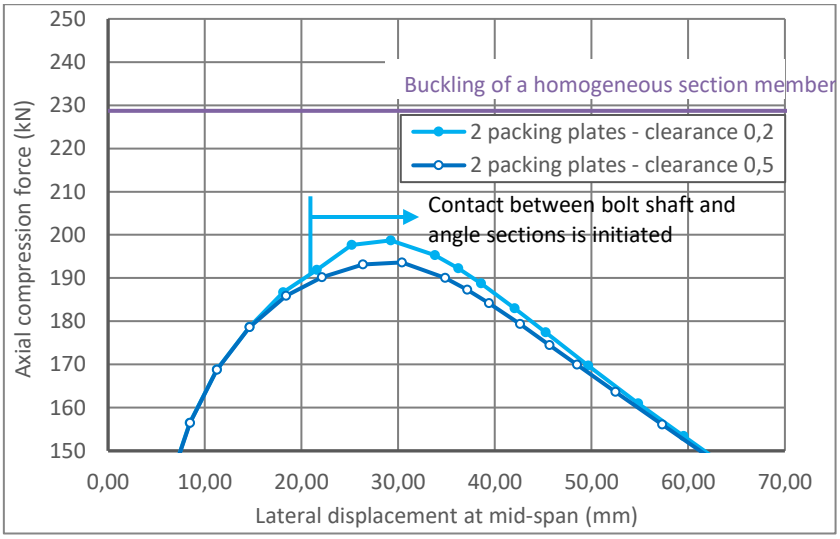

Figure 5.10: Influence of the bolt preloading – 20 packing plates

Finally, one may note that in practice the clearance is at least 1.0 mm for none fitted bolts. Therefore, it appears that members connected through none fitted bolts cannot be considered as perfectly connected if no measure is taken to prevent the sliding of the bolts, as for example the application of bolt preloading.

5.2.4 Influence of bolt preloading

Last, the members are analysed with bolted connections possessing a hole clearance of 2 mm but fabricated with a given value of pretension. The nominal preloading is calculated according to equation (1). In this equation $F_{p,CD}$ is the nominal preloading, f_{ub} is the tension resistance of the bolt and A_s is the stress area of the bolt.

$$F_{p,CD} = 0{,}7 f_{ub} A_s \quad (1)$$

The members are calculated with three levels of preloading as shown in Figure 5.11 and Figure 5.12 (20%, 60% and 100% of the full preloading obtained with equation (1)). Additionally, the stiffness of the connection is varied by considering three values of the friction coefficient (0.05, 0.3 and 0.5).
Figure 5.11 presents the results for members possessing 20 intermediate packing plates leading to a distance of $12.6i_{min}$ between each of them. One may observe that most of the members attain the reference resistance of a perfectly built-up member. It should be recalled that the same members calculated without preloaded bolts have only attained a resistance of approximatively 195 kN, i.e. 15% less (see Figure 5.5). Additionally, it appears that the value of the preloading and of the friction coefficient only influences little the buckling resistance. Only for a very low value of the friction coefficient and the preloading, a reduction of the buckling resistance may be observed. Nonetheless, even in this case, the resistance exceeds by approximatively 10% the resistance of members calculated without preloaded bolts.

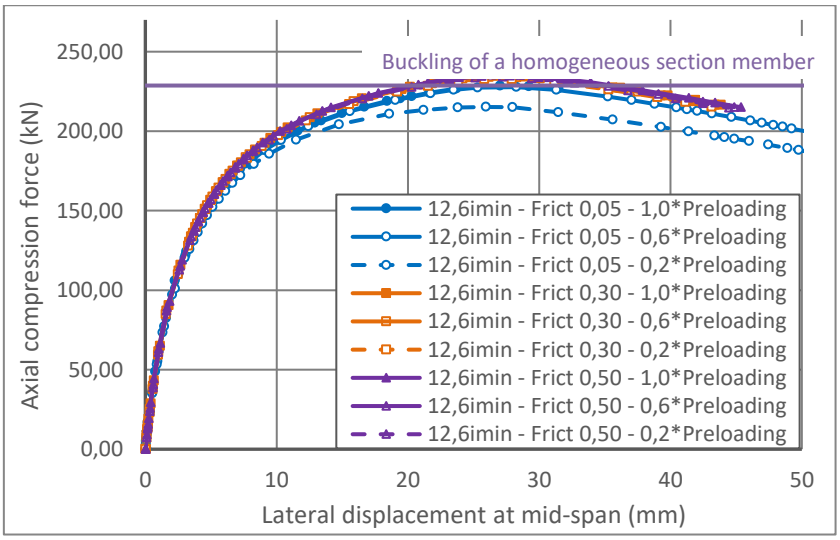

Figure 5.11: Influence of the bolt preloading – 20 packing plates

Finally, the members are calculated with only 2 intermediate packing plates and the results are presented in Figure 5.12 It can be observed that the value of the preloading and the friction coefficient has only a small influence on the buckling resistance. In case of members with only 2 intermediate packing plates (and therefore a high packing plate distance of $88i_{min}$) even a very high preloading combined with a very high value of friction coefficient only leads to a small increase of the resistance. It should however be noted that the members calculated with the highest preloading (the purple and orange curves of Figure 5.12) attain approximatively the resistance of members calculated with fitted bolts and 2 packing plates (see Figure 5.4). Inversely, the members with the lowest preloading (blue curves in Figure 5.11) appear to attain the lower bound resistance obtained for members with bolted connections possessing hole clearance (see for example Figure 5.5).

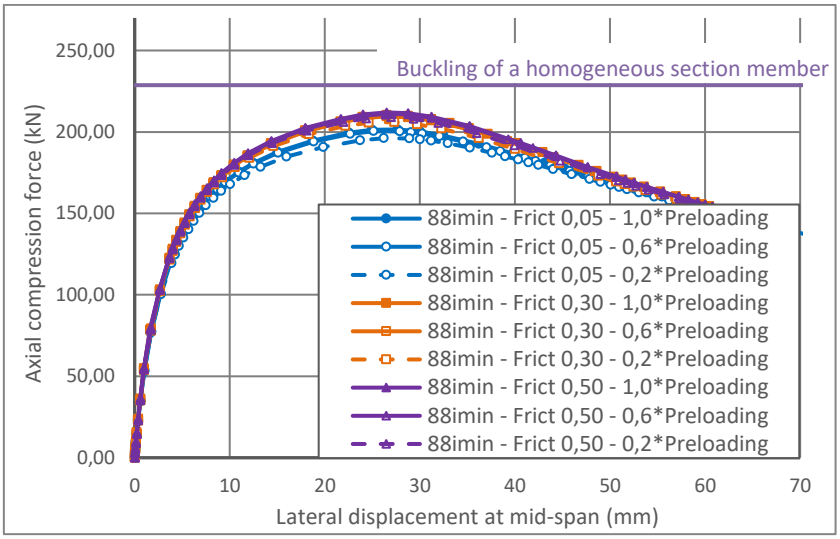

Figure 5.12: Influence of the bolt preloading – 2 packing plates

5.2.5 Influence of the member slenderness

Up to this point all members have been simulated with a length of 3600 mm leading to a theoretical relative slenderness of 1.50 (considering full connection). Hereafter, results are presented for different values of the relative slenderness and different packing plate distances. The relative slenderness is in the range between 0.25 and 2.50. Four different values of the packing plate distances are studied in Figure 5.13: $15i_{min}$, $30i_{min}$, $50i_{min}$ and $90i_{min}$. Figure 5.13 also represents buckling curve b of Eurocode 3 Part 1-1 as a reference. One should note that all members are connected with packing plates and fitted bolts (without clearance).

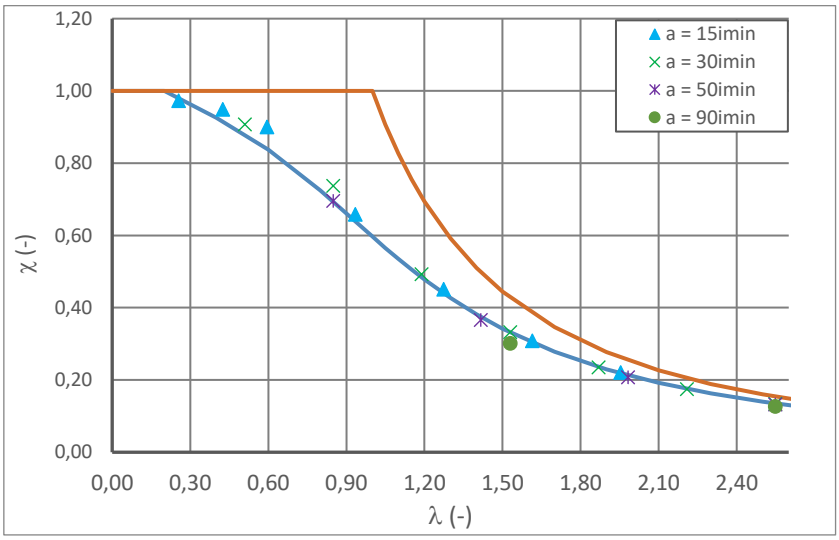

Figure 5.13: Influence of the slenderness

Figure 5.13 shows again that members possessing packing plate distances between $15i_{min}$ and $30i_{min}$ attain practically the same buckling resistance if the connection does not possess any clearance. One may observe a slight strength reduction for members with a packing plate distance of about $50i_{min}$. Yet, the difference vanishes for values of the relative slenderness

greater than approximatively 1.30. Additionally, Figure 5.13 indicates, not surprisingly, that the strength reduction is even higher for members with packing plate distances of $90i_{min}$. Nonetheless, the difference is relatively small (about 10%) for a relative slenderness of approximatively 1.50. For lower values of the relative slenderness, the difference may probably increase. However, owing to the high packing plate distance, the total member length and hence the relative slenderness is also high for the built-up member even if only two intermediate connections are used.
Finally, one may note that the results represented in Figure 5.13 confirm the conclusions of the sub-study presented in paragraph 5.2.2. In fact, if the connection is sufficiently rigid (bolted packing plate connections without clearance or packing plate connections with pre-loaded bolts), a noticeable buckling strength reduction only occurs for high distances between packing plates.

5.3 Scope of the numerical simulations

5.3.1 BBE specimens

The field of parameters is chosen according to the conclusions of the sensitivity study. In particular, Table 5.1 shows that different values of the packing plate spacing are considered. Additionally, the connection type is included in the parametric study. Finally, the influence of the yield stress is accounted for by studying steel grades S235, S355 and S460.

Table 5.1: Field of the parametric study

Parameter	Value
Cross section	L70x70x7 L150x150x15
Packing plate thickness	$t_{Section}$
Packing plate distance	$15i_{min}$, $30i_{min}$, $50i_{min}$, $75i_{min}$
Member slenderness	0.4 – 2.0
Bolt pretension	0, 10% of nominal preloading, 100% of nominal preloading
Bolt diameter	According to recommendations for each section
Type of bolts	Fitted bolts, Snug tight bolts, preloaded bolts
Steel grades	S235, S355, S460
Loading	Axial force

5.3.2 SBE and SBU specimens

The field of the parametric study for SBE and SBU specimens is also chosen based on the sensitivity study. However, additionally to the general geometric parameters, the influence of the angle size difference in case of SBU members is studied. Also, SBE and SBU members are studied under the combined influence of bending and axial compression.

Table 5.2: Field of the parametric study

Parameter	Value
Cross section	2L70x70x7 (SBE70) 2L150x150x15 (SBE150) L90x90x9+L60x60x6 (SBU90+60) L150x150x15+L80x80x8 (SBU150+80)
Packing plate thickness	$=t_{Section}$ (in case of SBU minimum thickness)
Packing plate distance	$30i_{min}$, $50i_{min}$, $70i_{min}$, $90i_{min}$
Member slenderness	0.4 – 2.0 (5 values)
Bolt pretension	0, 10% of nominal preloading, 100% of nominal preloading
Bolt diameter	According to recommendations for each section
Type of bolts	Fitted bolts, Snug tight bolts, preloaded bolts
Steel grades	S235, S355, S460
Loading	Axial force, Axial force + bi-axial bending (10 combinations)

6 Outlook

The objective of Deliverable 3.3 was to give a detailed description concerning the validation of the numerical model and to define the scope of the parametric study. The results of the parametric study will be presented in Deliverable 3.4 together with the development of the design proposal for closely spaced built-up members.

References

[1] Kitipornchai, S., Lee, H. W. (1986), "Inelastic Experiments on Angle and Tee Struts", Journal of Constructional Steel Research, Vol. 6, 219-236.
[2] Zhang L, Jaspart JP, Stability of members in compression made of large hot-rolled and welded angles, Université de Liège, 2013.

List of Figures

List of Tables